

1 **Development and performance of a high-resolution surface wave and storm surge forecast model: Application**
2 **to a large lake**

3 **Laura L. Swatridge¹, Ryan P. Mulligan¹, Leon Boegman¹, and Shiliang Shan^{1,2}**

4 ¹ Department of Civil Engineering, Queen's University, Kingston, ON, Canada, K7L 3N6.

5 ² Department of Physics and Space Science, Royal Military College of Canada, Kingston, ON, Canada,
6 K7K 7B4.

7 Correspondence to: Laura Swatridge (l.swatridge@queensu.ca)

8

9 **Key Points:**

- 10 • A real-time forecast model of wind-driven hydrodynamics in Lake Ontario is developed.
- 11 • Model performance compares well with observed data and other forecast models.
- 12 • Forecast lead time impacts the accuracy of wave height and storm surge predictions.

13 **Abstract**

14

15 A real-time forecast model of surface hydrodynamics in Lake Ontario (Coastlines-LO) was developed to
16 automatically predict storm surge and surface waves. The system uses a dynamically coupled Delft3D –
17 SWAN model with a structured grid to generate 48 h predictions for the lake that are updated every 6 h.
18 The lake surface is forced with meteorological data from the High Resolution Deterministic Prediction
19 System (HRDPS). The forecast model has been running since May 2021, capturing a wide variety of storm
20 conditions. Good agreement between observations and modelled results is achieved, with root mean squared
21 errors (RMSE) for water levels and waves under 0.02 m and 0.26 m, respectively. During storm events, the
22 magnitude and timing of storm surges are accurately predicted at 9 monitoring stations (RMSE < 0.05 m),
23 with model accuracy either improving or remaining consistent with decreasing forecast length. Forecast
24 significant wave heights agree with observed data (1-12% relative error for peak wave heights) at 4 wave
25 buoys in the lake. Coastlines-LO forecasts for storm surge prediction for two consecutive storm events were
26 compared to those from the Great Lakes Coastal Forecasting System (GLCFS) to further evaluate model
27 performance. Both systems achieved comparable results with average RMSEs of 0.02 m. Coastlines-LO is
28 an open-source wrapper code driven by open-data and has a relatively low computational demand,
29 compared to GLCFS, making this approach suitable for forecasting marine conditions in other coastal
30 regions.

31

32 **1 Introduction**

33

34 Coastal regions of large lakes can face hazardous conditions with costly consequences due to strong storm
35 events, where powerful winds generate large waves and storm surge (Danard, 2003; FEMA, 2014;
36 Gallagher et al., 2020). Waves during these events can cause erosion, overtopping, and run-up, with the
37 hazards being greater when the water level is elevated from storm surge. The intensity and frequency of
38 strong storm events is increasing in the Great Lakes region as a result of climate change, as tropical storms
39 are predicted to reach higher latitudes more often (Bender et al., 2010; Studholme et al., 2022). In addition,
40 the mean water levels in the Great Lakes are being impacted by climate change, with large seasonal
41 fluctuations in lake levels and record low and high water levels consistently occurring in recent years
42 (Gronewold and Rood, 2019). The combined impacts of these projections present a greater risk for
43 hazardous conditions in Great Lakes coastal regions, and developing better methods to understand and
44 model the physical processes occurring during storms is important to help mitigate the risk. (Chisholm et
45 al., 2021; Gronewold et al., 2013).

46
47 ‘Real-time forecasting’ of lakes and coastal oceans can be achieved by applying numerical models to run
48 predictive simulations of future hydrodynamic conditions in real time. Water level, circulation, and
49 temperature simulations, using forecast models of large lakes and reservoirs, aid in water quality
50 management (Baracchini et al., 2020; Carey et al., 2021; Lin et al., 2022). Coastal hazard forecasting is also
51 being applied in numerous ocean regions, including the northern Gulf of Mexico where forecast systems of
52 water levels and waves predict hurricane impacts on various scales (Bilskie et al., 2022; Dietrich et al.,
53 2018; Paramygin et al., 2017). Similarly, Rey and Mulligan (2021) use a coupled Deflt3D–SWAN model
54 to forecast storm conditions in coastal North Carolina, investigating the influence of various atmospheric
55 forecast models on the results during hurricanes. Specific to lakes, the National Oceanic and Atmospheric
56 Administration (NOAA) has implemented forecast models for North American coastal regions, including
57 the Great Lakes, with the Great Lakes Coastal Forecast System (GLCFS). The GLCFS uses a high-
58 resolution (30 m – 2 km) hydrodynamic model (FVCOM) to simulate physical processes including currents,
59 temperatures, and water levels (Kelley et al., 2018; Peng et al., 2019). Waves in the Great Lakes are
60 predicted by Environment and Climate Change Canada’s (ECCC) Regional Ensemble Wave Prediction
61 System (REWPS), which uses a probabilistic approach to forecast wave characteristic 3 days into the future.

62
63 Developing deterministic forecast models that run in real-time requires dealing with the challenge of
64 minimizing the computational runtime of the model while still achieving accurate results (model resolution
65 and performance), as the forecasts must be available in advance of the actual event. This need to effectively
66 balance efficiency and accuracy in real-time models is an active research area (Elko et al., 2019). In
67 addition, clear and efficient dissemination of forecasts must be provided to users and stakeholders. Typical
68 real-time coastal models require large computing resources to run high resolution and accurate forecast
69 simulations (Bilskie et al., 2022; Kelley et al., 2018), while fewer model applications focus on developing
70 flexible systems that can achieve accurate results while running on local computers, often for smaller
71 domains, using open data and with a smaller computational allowance (Lin et al., 2022; Rey and Mulligan,
72 2021).

73
74 The accuracy of numerical models for simulating the hydrodynamic response of coastal regions to storm
75 events has increased with advances in computing power, data availability, and the development of models
76 that can better represent more physical processes and their interactions, however model performance is still
77 limited by the quality of input and forcing data available for a simulation. Model ability also depends on
78 the grid resolution, with higher resolution models being more capable of resolving bathymetric features
79 (Bilskie et al., 2022), and the inclusion of relevant processes, such as wave-current interactions and

80 baroclinic effects (Asher et al., 2019; Swatridge et al., 2022). A main consideration is the accuracy of the
81 atmospheric forcing, as winds are the primary driver of surface behaviour, and errors in the winds translate
82 through as errors in the modelled results (Dietrich et al., 2018; Farhadzadeh and Gangai, 2017; Rey and
83 Mulligan, 2021).

84
85 A probabilistic approach can be used to account for uncertainty in atmospheric forcing by running multiple
86 variations of the same event, however this requires large computational resources (Baracchini et al., 2020;
87 Fleming et al., 2008). In deterministic forecasts of water levels in Lake Erie, error in the atmospheric forcing
88 was significantly larger for 240 h forecasts compared to the 120 h forecasts, which translated to increased
89 error in predicted water levels (Lin et al., 2022). The longer forecast predicted excessive seiching and an
90 underestimation in peak water level, which improved as forecast length decreased. Forecasts of hurricane
91 storm surge and waves in the Gulf of Mexico by Forbes et al. (2010), Dietrich et al. (2018), and Bilskie et
92 al. (2022) found trends of decreasing error in storm surge prediction with shorter forecast length. Longer
93 forecasts (~5 days) resulted in storm surge variations of up to 4 m from the best track predictions, attributed
94 to variability in atmospheric forcing, and for forecasts shorter than 2.5 days, simulations converged on a
95 solution, and error was almost constant (Dietrich et al., 2018).

96
97 The hydrodynamics of Lake Ontario have been simulated on various scales in previous studies (e.g., Huang
98 et al., 2010; Paturi et al., 2012; Prakesh et al., 2007; Shore, 2009). Numerical models have also been used
99 to simulate waves and circulation during extreme events in the Kingston Basin (Cooper and Mulligan, 2016;
100 McCombs et al., 2014a; McCombs et al., 2014b). Sogut et al. (2019) used a combination of analyzing
101 historical water level and wave data, as well as numerical modelling of extreme storm events to gain insight
102 on lake seiching, storm surges, and wave patterns. Historical data have also been studied to determine the
103 risk of flooding due to storm surge along the Lake Ontario shoreline with a statistical model (Steinschneider,
104 2021). Surface waves and storm surge were simulated over the entire lake by Swatridge et al. (2022) during
105 recent storm events. Their study investigated the influence of different wind fields on the accuracy of storm
106 surge simulation, finding that variations in meteorological forcing were the primary source of uncertainty
107 in model results.

108
109 In the present study, an existing depth-averaged numerical model of Lake Ontario (Swatridge et al., 2022)
110 was applied to the lake to forecast water levels and waves in real-time, driven by spatially varied wind
111 fields from a high-resolution wind forecast model. The workflow develops an open-source Python- and
112 MATLAB-based wrapper code, that has been successfully applied to other systems using different
113 hydrodynamic models as part of the Canadian Coastal and Lake Forecasting Model System (Coastlines;

114 <https://coastlines.engineering.queensu.ca>; Lin et al., 2022; Rey and Mulligan, 2021). This flexible
115 methodology uses open access forcing/validation data and requires a relatively low computational demand,
116 compared to other existing Great Lakes storm surge models, allowing for application to other locations.
117 Model performance is evaluated by comparing results to near-real time observed data. Forecast results, for
118 storm surges and waves are statistically investigated over forecast lead times ranging from 6 to 48 h.

119

120 **2 Methods**

121

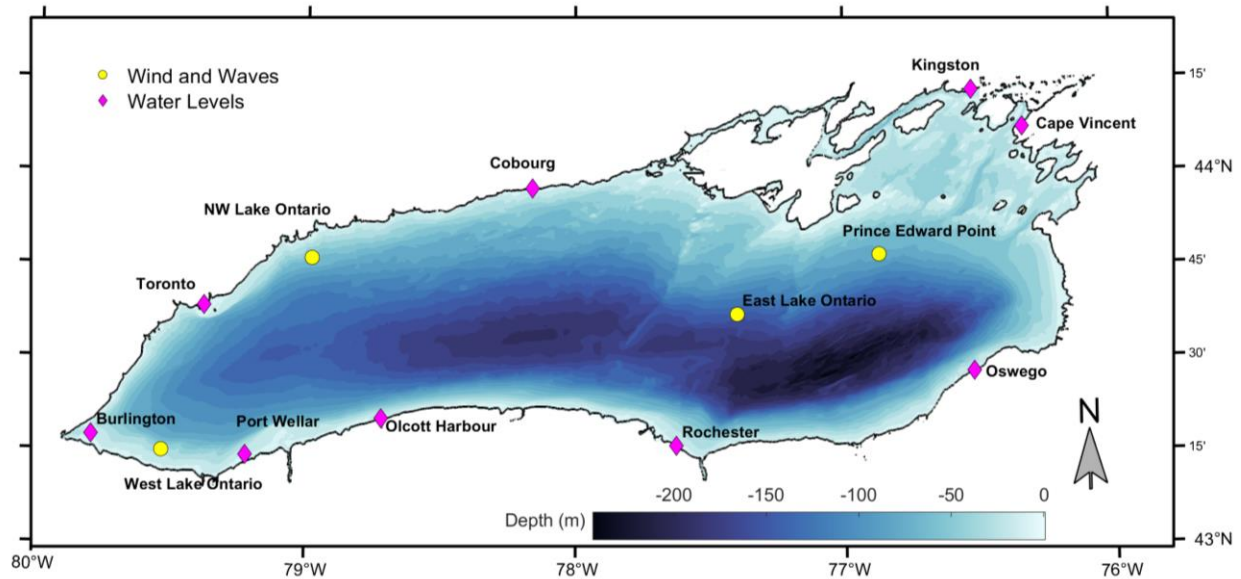
122 *2.1. Modelling Approach*

123 A two-dimensional (depth-averaged) coupled hydrodynamic-wave model is applied to Lake Ontario to
124 simulate wind driven hydrodynamics and waves using Delft3D-SWAN. The Delft3D flow model calculates
125 non-steady flow on a structured grid by solving the Reynolds-Averaged Navier Stokes equations (Lesser et
126 al., 2004). Wave conditions are simulated with the phase-averaged wave model, Simulating Waves
127 Nearshore (SWAN), which uses the spectral action balance equation to compute random wind-generated
128 waves. SWAN accounts for non-linear wave interactions, wave propagation, refraction, dissipation due to
129 whitecapping, bottom friction and depth-induced breaking (Booij et al., 1999). The models are dynamically
130 coupled to account for wave-current interactions. Radiation stress gradients from SWAN simulations are
131 input into the horizontal momentum equations in Delft3D to account for the impacts of waves on
132 circulation, such as wave-induced mass fluxes driving currents, and enhanced bed shear stress. Results from
133 the hydrodynamic simulation are then used to update water levels and circulation in the wave model.

134

135 Model setup choices were made based on simulations by Swatridge et al. (2022) which were adapted for
136 the present study to minimize computational demand, allowing the system to run in real-time. The Delft3D
137 simulation uses a curvilinear grid with a horizontal resolution gradually ranging from 250-450 m. The wave
138 grid has a coarser resolution, ranging from 350-600 m, thus reducing the computational time required to
139 complete a wave simulation while still achieving higher resolution in nearshore areas (Table S2 in the
140 supplementary material). Flow simulations are depth-averaged and barotropic, shown by Swatridge et al.
141 (2022) to accurately represent surface storm surge in Lake Ontario, with root mean squared errors (RMSEs)
142 between observations and model results ranging between 0.01 m - 0.07 m during several major events.
143 Bathymetry data was interpolated to the grid from the US National Centers for Environmental Information's
144 (NCEI) 3-arcsecond (~ 90 m) resolution dataset with supplementary data from the ETOPO1 global relief
145 model with a resolution of approximately 1.3 km (Fig. 1). Detailed sensitivity testing for this model was
146 completed in Swatridge et al. (2022) to calibrate model parameters. Hydrodynamic simulations use a time

147 step of 120 s to satisfy the Courant–Friedrichs–Lewy stability criterion, and coupling with the stationary
148 wave model occurs every 60 minutes.

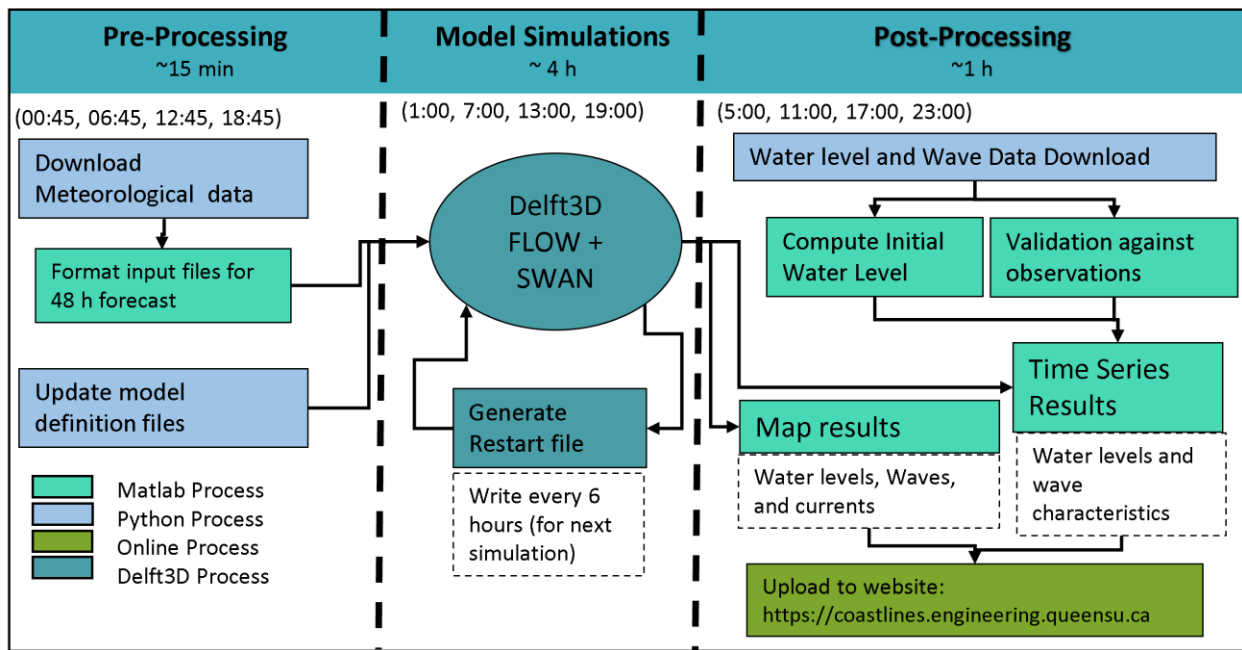


149
150 **Figure 1:** Map of Lake Ontario showing NCEI bathymetry and the location of real-time water level, wind,
151 and wave observation stations (Table 1, Table 2)

152
153 Spatially varied atmospheric input from the Meteorological Service of Canada (MSC) High Resolution
154 Deterministic Prediction System (HRDPS) is used to drive the model (Milbrandt et al., 2016). HRDPS is
155 an hourly assimilated forecast system downscaled from the larger scale Regional Deterministic Prediction
156 System (RDPS) that provides hourly predictions of surface pressure and wind velocity components with a
157 horizontal resolution of 2.5 km for the pan-Canada domain. The system runs every 6 h, predicting
158 atmospheric conditions 48 h into the future. This wind-forcing was successfully used by Swatridge et al.
159 (2022) to simulate the lake surface response to a range of storm conditions. Their modelled results for water
160 levels and surface waves agreed with observations at up to 16 locations in Lake Ontario, resulting in
161 maximum difference between predicted and observed peak wave heights and water levels of 0.4 m and
162 0.08 m, respectively. No lateral boundary conditions are applied to account for the influence of the riverine
163 flows (Niagara and St. Lawrence Rivers), as results from previous modelling studies have concluded that
164 the hydrodynamic influence of river inflows and outflows is limited to within 10 km of the river mouth,
165 and therefore can be neglected for simulations of lake wide water level over event based timescales.
166 (Prakash et al., 2007; McCombs et al. 2014a). The closed based approach leads to uncertainties in the
167 simulated results in the river region, however the impacts on the lake-wide hydraulics is expected to be
168 minimal.

170 2.2. Development of an Automated Prediction System

171 The forecast system uses a combination of code written in MATLAB and Python to automatically run every
 172 6 h and has been operational since May 2021 (<https://coastlines.engineering.queensu.ca/lake-ontario/>). The
 173 workflow (Fig 2) consists of pre-processing, model simulation and post processing stages. For pre-
 174 processing, initiation of the modelling system is scheduled to occur when a new HRDPS forecast becomes
 175 available. Python is used to download the latest forecast and MATLAB is used to automatically process the
 176 atmospheric forcing and write input files for Delft3D-SWAN. The Delft3D model definition files are then
 177 updated with the correct time information.



178
 179 **Figure 2.** Diagram of the automated workflow for processes performed for each model cycle (every 6 h
 180 initiated by Windows Task Scheduler) on the local Coastlines server.

181
 182 Model simulations cover a period of 48 h and are ‘hot-started’ with a restart file from a previous model run
 183 if available. If a restart file is not available, simulations begin from rest with initial water levels of 0 m and
 184 current speeds (u) of 0 m s^{-1} throughout the lake. When the simulation finishes, all available real-time
 185 observed data, outlined in Table S1 in the supplementary material, is downloaded using Python, which is
 186 then processed in MATLAB. Observed water levels at each station are averaged over the previous 12 h and
 187 used to locally adjust the datum of the model outputs. We acknowledge that assimilating observed water
 188 levels into the initial conditions may be a preferred approach, but this is beyond the scope of the present
 189 study and may be incorporated into future versions on Coastlines-LO. The model simulates high frequency
 190 variability in water levels generated by winds. Seasonal changes in water levels due to inflows, outflows,
 191 and evaporation are not included, but are accounted for in post-processing.

192
 193 Time series plots of observed water levels and wave heights are automatically compared to the forecast
 194 model results from the previous 2.5 days at the observation locations and additional plots are created to
 195 provide predictions at other locations of interest with no observed data (Fig. 1). Spatial snapshots of model
 196 results across the lake are generated at select times, as well as animations showing key output parameters
 197 during the forecast simulation. All outputs are exported to Google Sheets and displayed on the project
 198 webpage, <https://coastlines.engineering.queensu.ca/>. The system runs in a Windows environment using 16
 199 cores of a 32-core XEON workstation, with each workflow cycle taking approximately 5 h to complete a
 200 48 h forecast simulation.

201
 202 *2.3. Real-time Comparison between Model Results and Observations*

203 Near real-time observations of water surface elevation (η) data are available at 9 water level gauges around
 204 the perimeter of Lake Ontario from the National Oceanic and Atmospheric Administration (NOAA) and
 205 the Department of Fisheries and Oceans Canada (DFO), with temporal resolutions of 3 minutes and 6
 206 minutes, respectively (Fig. 1; Table 1). Hourly surface waves and winds are measured in Lake Ontario at
 207 one US National Data Buoy Center (NDBC) buoy and ECCC buoys from spring to early winter (Table 2).
 208 The buoys report the significant wave height (H_s), peak wave period (T_p), surface wind speed and direction
 209 averaged over an 8-minute period (U).

210
 211 **Table 1:** List of real-time water level gauge station locations

Name	Longitude	Latitude	Source
Oswego	-76.52	43.46	NOAA
Rochester	-77.63	43.27	NOAA
Olcott Harbour	-78.72	43.34	NOAA
Cape Vincent	-76.33	44.12	NOAA
Port Wellar	-79.22	43.24	DFO
Cobourg	-78.16	43.96	DFO
Burlington	-79.79	43.29	DFO
Kingston	-76.52	44.22	DFO
Toronto	-79.38	43.64	DFO

213 **Table 2:** List of real-time wave buoy locations

Name	Longitude	Latitude	Depth	Source
Prince Edward Point	-76.87	43.78	68 m	ECCC
West Lake Ontario	-79.53	43.25	35 m	ECCC
Northwest Lake Ontario	-78.98	43.77	54 m	ECCC
East Lake Ontario	-77.40	43.62	140 m	NDBC

214

215 For long term analysis of results, the residual component of the water level data, representing storm surge,
 216 is isolated at the gauge locations by finding the difference between the total water level and the average
 217 water level, calculated using a gaussian window of 7 days (Steinschneider et al., 2021). Model performance
 218 is quantified using statistical measures including the RMSE (eq. 1), normalized RMSE (NRMSE; eq. 2),
 219 and the correlation coefficient (r; eq. 3):

$$220 \quad RMSE = \sqrt{\frac{\sum_{i=1}^n (x_i - y_i)^2}{n}} \quad (1)$$

$$221 \quad NRMSE = \frac{RMSE}{\bar{y}} \quad (2)$$

$$222 \quad r = \frac{\sum (y - \bar{y})(x - \bar{x})}{\sqrt{\sum (y - \bar{y})^2 \sum (x - \bar{x})^2}} \quad (3)$$

223 Where x_i and y_i ($i = 1, 2, 3, \dots N$) are time series of modelled and observed data respectively, and N is the
 224 number of samples in the series. Storm surge events are identified from the water level data using the peaks-
 225 over-threshold method (Steinschneider et al. 2021). Forecast error during select events was evaluated by
 226 computing error metrics for consecutive forecasts leading up to the peak of the event. For each forecast, the
 227 relative error (RE; eq. 4), between observed and simulated maximum storm surge relative to the mean water
 228 level calculated at water level gauge locations, and between observed and modelled maximum wave heights
 229 at buoy locations was computed. The RMSE for each location was computed over a 6 h period that included
 230 the peak of the event.

$$231 \quad RE = \frac{|(\bar{y} - y) - (\bar{x} - x)|}{(\bar{y} - y)} \quad (4)$$

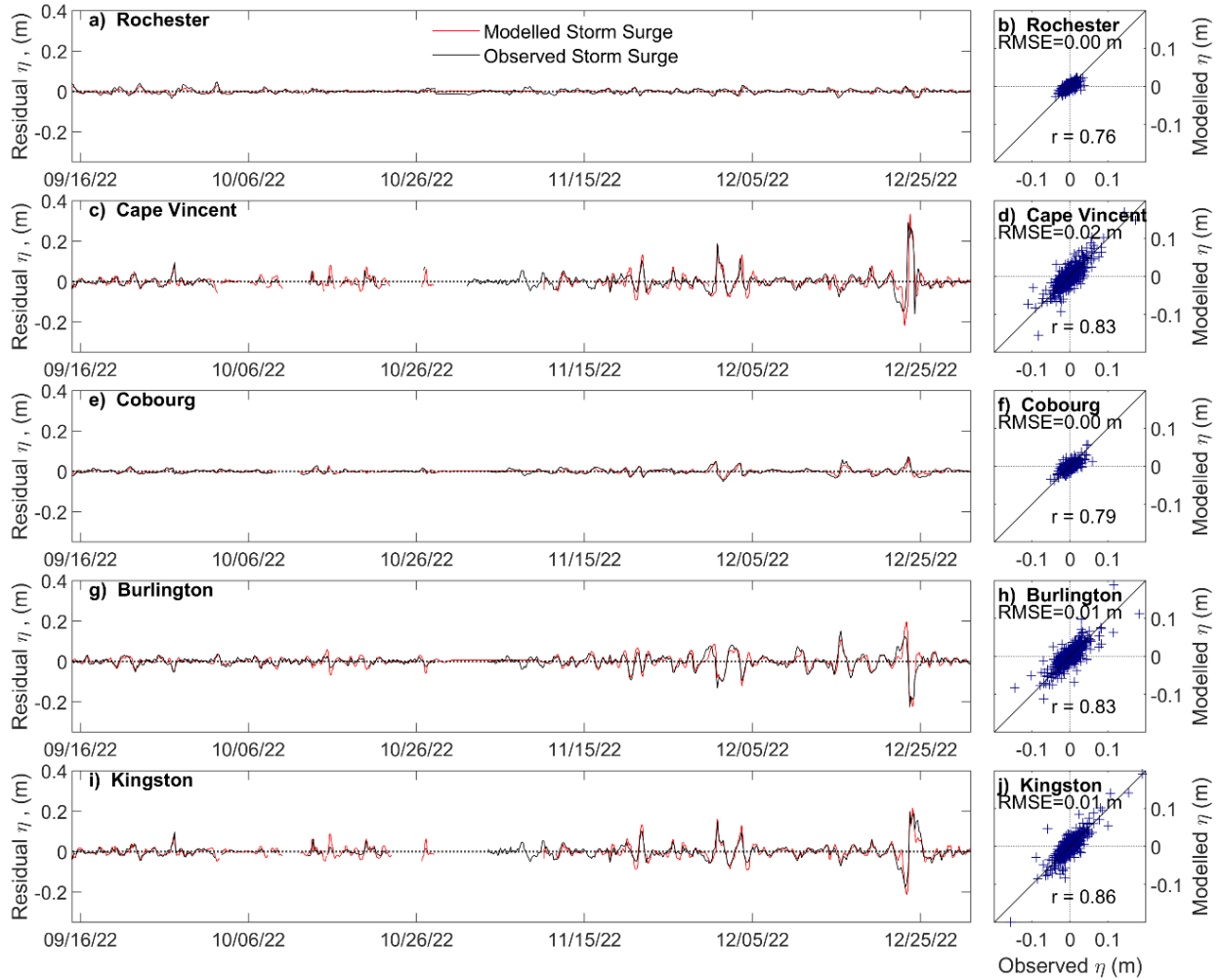
232

233 **3 Results**

234

235 *3.1. Long-term model performance*

236 Simulation results, for water levels and waves, at the observation locations, were compiled over the 20-
237 month operational period. The first 6 h of each 48 h forecast were stitched into a single time series, and
238 these results were compared to the observed data (Fig. S1 in the supplementary material). During this time,
239 seasonal changes in the observed mean lake level fluctuated by over 1 m, with the highest water levels
240 occurring in May 2022. The ability of the model to reproduce storm surge was investigated over a four-
241 month period when multiple storm events occurred (106 days from 15 September 2022 to 30 December
242 2022; Fig. 3). Stations with larger ranges of observed water levels (i.e., Burlington, Cape Vincent), located
243 at the east and west ends of the lake (i.e., Fig. 3c, g) show a slight bias, where the model tended to slightly
244 overpredict the maximum and minimum values, corresponding to larger RMSE values (Table 3). These
245 stations also tended to show a stronger correlation ($r = 0.83 - 0.86$); whereas observation points with
246 typically smaller ranges in water levels (Fig. 3a, e) resulted in weaker correlations ($r = 0.76 - 0.79$).
247 Normalized results show comparable error statistics at all stations, with larger errors occurring at locations
248 with smaller storm surges (i.e., Rochester, Oswego).
249



250

251 **Figure 3:** Observed (black) and modelled (red) residual water levels at select observation points over a 3
 252 month period (September – December 2022) with corresponding scatter plots and error statistics over this
 253 period at select locations.

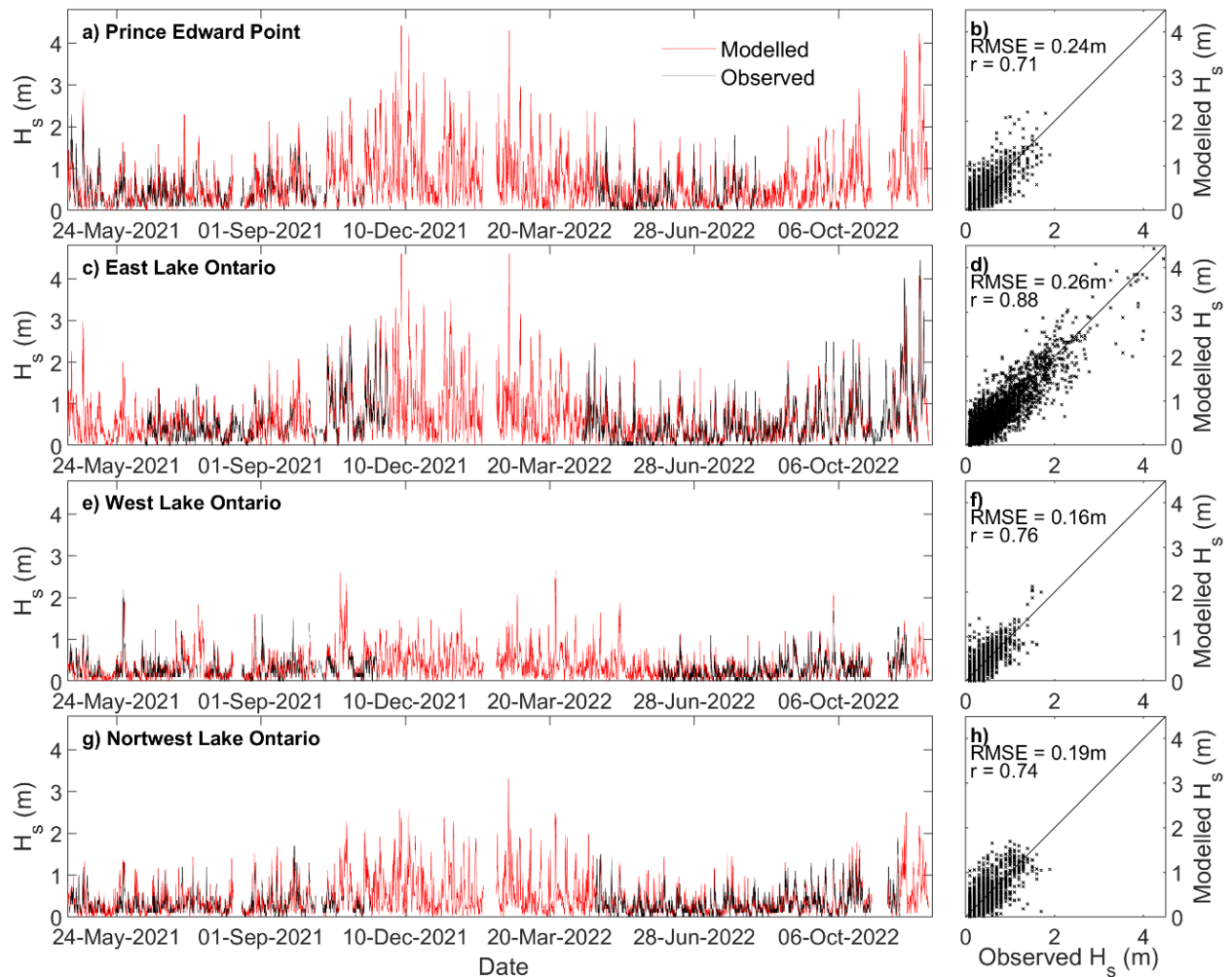
254

255 **Table 3:** Error Statistics for residual water level results over 106 days (September 15 – December 30, 2022)

	Minimum η (m)	Mean η (m)	Maximum η (m)	RMSE (m)	NRMSE (m)	r
Oswego	-0.10	0.07	0.12	0.01	0.15	0.80
Rochester	-0.03	0.03	0.04	0.00	0.16	0.76
Olcott	-0.16	0.04	0.11	0.01	0.19	0.80
Cape Vincent	-0.22	0.10	0.34	0.02	0.16	0.83
Port Wellar	-0.19	0.06	0.16	0.01	0.14	0.86
Cobourg	-0.08	0.04	0.07	0.01	0.14	0.79
Toronto	-0.16	0.07	0.14	0.01	0.14	0.83
Burlington	-0.22	0.10	0.20	0.02	0.14	0.83
Kingston	-0.21	0.09	0.25	0.01	0.14	0.86

256
 257 Results for simulated H_s at buoy locations show the largest waves occurred during winter, between
 258 December and March (Fig.4). Results showing forecasted wave period compared to observations are shown
 259 in Fig S2 in the supplementary material. Over the 600-day operational period, no monitoring data was
 260 available for comparison and Lake Ontario could potentially experience partial ice-cover in nearshore areas,
 261 impacting the wave environment (Anderson et al., 2018). Stations in the eastern end of the lake (Prince
 262 Edward Point, East Lake Ontario) are expected to experience the largest waves due to the prominent north-
 263 easterly direction of storms over the lake, which results in winds blowing along the long-axis of the lake
 264 creating a large fetch at these locations (Lacke et al. 2007; McCombs et al. 2014a). Error statistics show
 265 similar values for RMSE at these points however Prince Edward Point had the lowest correlation coefficient
 266 (Fig. 4a, b; $r = 0.71$), while East Lake Ontario showed the highest correlation (Fig. 4c, d; $r = 0.88$). Lower
 267 RMSE were at stations with smaller waves (Fig. 4e, g), and normalized results (Table 3) show comparable
 268 results at all buoys (NRMSE = 0.42 – 0.53 m).

269



270

271 **Figure 4:** Time series of observed (black) and modelled (red) significant wave height over the duration that
 272 the buoys were in the lake (September -December 2022) with corresponding error scatter plots at the
 273 location of the 4 buoys. Note that the model was offline and are unavailable between February 9 – 27, 2022
 274 due to a change of service for the meteorological inputs.

275

276 **Table 3:** Error statistics for significant wave heights at the buoy locations over 600 days (April 21, 2021 –
 277 December 12, 2022)

Location	Mean H_s (m)	Maximum H_s (m)	RMSE (m)	r	NRMSE (m)
Prince Edward Point	0.44	3.82	0.24	0.71	0.53
East Lake Ontario	0.62	4.42	0.26	0.88	0.42
West Lake Ontario	0.34	2.60	0.16	0.76	0.48
Northwest Lake Ontario	0.35	2.29	0.19	0.74	0.53

278

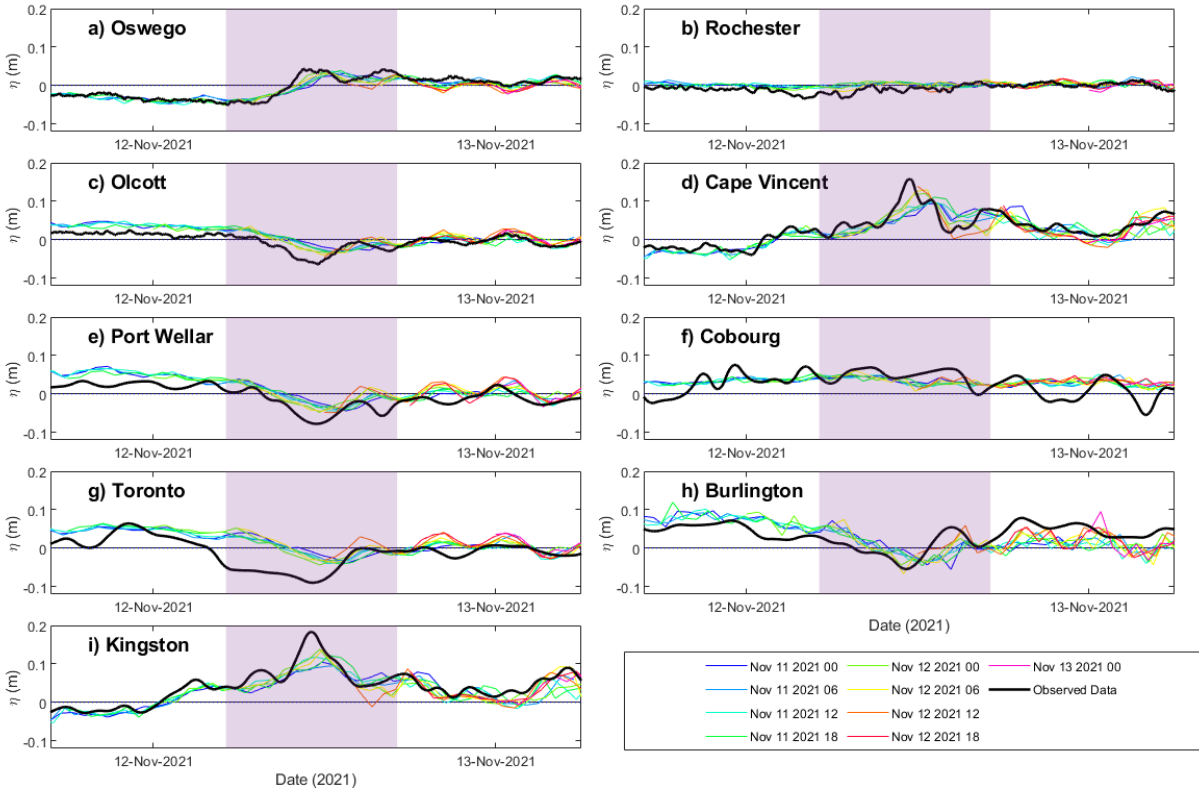
279 *3.2. Storm event forecasts*

280 The performance of the model was evaluated over an event on November 11- 12 2021, consisting of wind
 281 speeds that approached 15 m s⁻¹, with the direction rotating clockwise from blowing towards the northeast
 282 to the winds dominantly blowing towards the east over a 24 h period. This event was selected due to the
 283 large storm surge generated ($\eta = 0.17$ m), and it resulted in the largest significant wave height that occurred
 284 over the 20 month operational period with wave measurements available at all buoy locations for
 285 comparison. Overlapping 48 h HRDPS forecasts (i.e., generated every 6 h) were validated against buoy
 286 observations, with good agreement found between modelled and predicted total wind speeds and directions,
 287 with peak wind speeds underrepresented by at most, 4.21 m s⁻¹ at Northwest Lake Ontario and overpredicted
 288 by up to 2.61 m s⁻¹ at Prince Edward Point (Fig. S3 in the supplementary material)

289

290 This event resulted in an observed storm surge of up to 0.16 m in the northeast region of the lake, at Cape
 291 Vincent and Kingston. The forecast simulations captured the timing and magnitude of the event peak, with
 292 predicted surge values ranging between 0.12 m – 0.17 m (Fig.5d, i). A set down of about 0.10 m was
 293 recorded at the Burlington station, which was underpredicted by the model by up to 0.05 m for the initial
 294 forecast results, and improves as the forecast lead time decreases, to a prediction of 0.08 m. The simulated
 295 results at this location predicted water levels up to 0.05 m higher than the observations for the 24 h preceding
 296 the storm (Fig.5h). Notable error can also be identified at Cobourg (Fig. 5f) with the model predicting
 297 negligible fluctuations in the water surface, but observations show some oscillations (0.05 m).

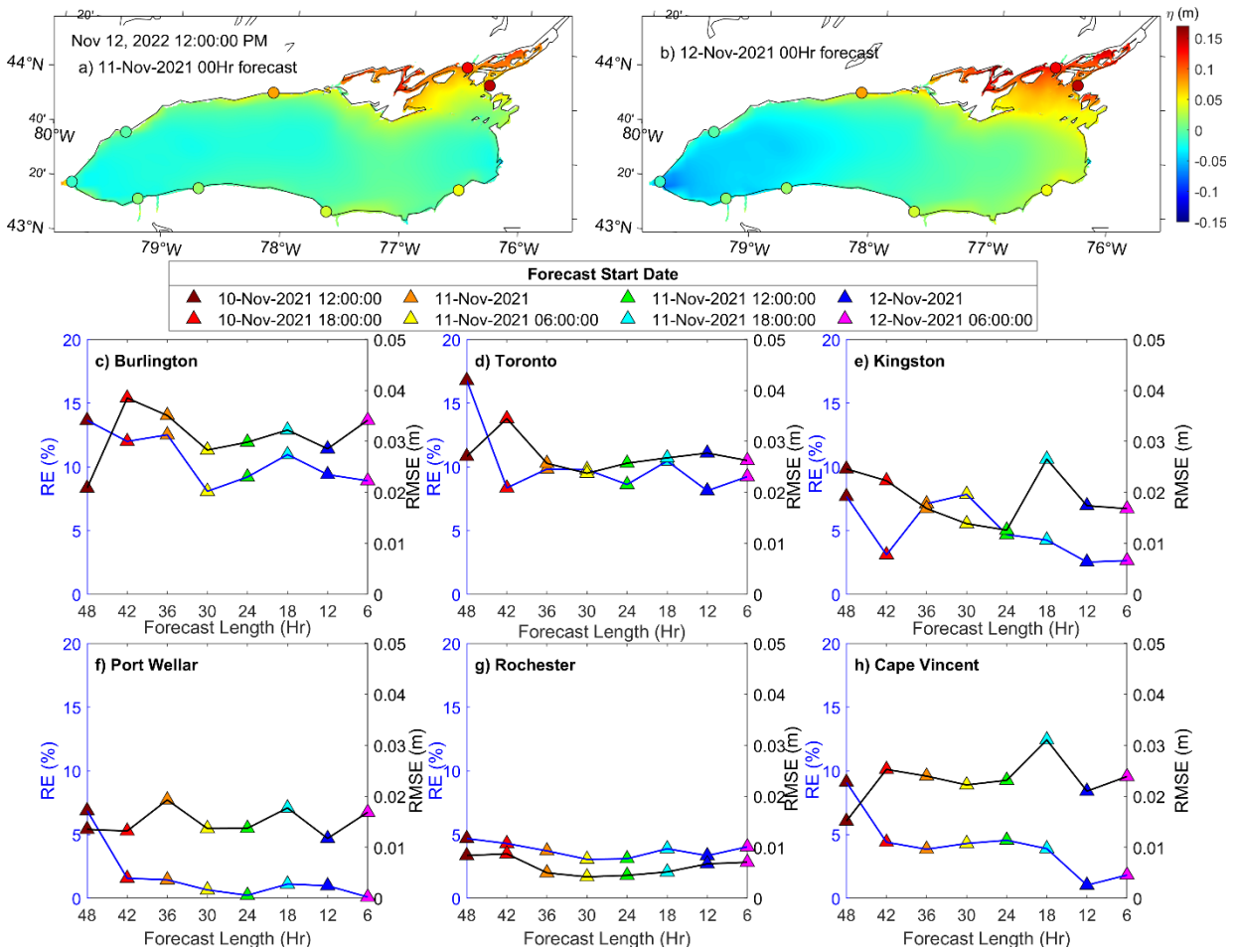
298



299
 300 **Figure 5:** Time series of measured water levels at various observation points compared to forecasted data
 301 from progressive model simulations. The highlighted area indicates the 12 h period over which error
 302 statistics are computed.

303
 304 Forecast performance was quantified by computing error statistics, over the duration of the event, for each
 305 forecast leading up to the time of peak water level. The largest errors occurred at the location of the set
 306 down, Burlington and Toronto, with a nearly constant RMSE of 0.03 m, and RE of 14% and 10%
 307 respectively (Fig. 6c, d). The errors at all stations remained fairly constant with RMSE and RE under 0.03 m
 308 and 10%, respectively, for each new forecast. However, map results showing the spatial variability in water
 309 level predictions from forecasts 12 h and 36 h before the storm peak show large differences (Fig. 6a,b). The
 310 earlier results (Fig. 6a) simulated a far less extensive storm surge in the northeast region of the lake than
 311 what was subsequently predicted 24 h later (Fig. 6b), when the storm surge was simulated to impact most
 312 of the northeast shoreline. The later forecast also predicted spatially larger set-down, about 0.10 m more
 313 than the earlier forecast in the western region of the lake.

314

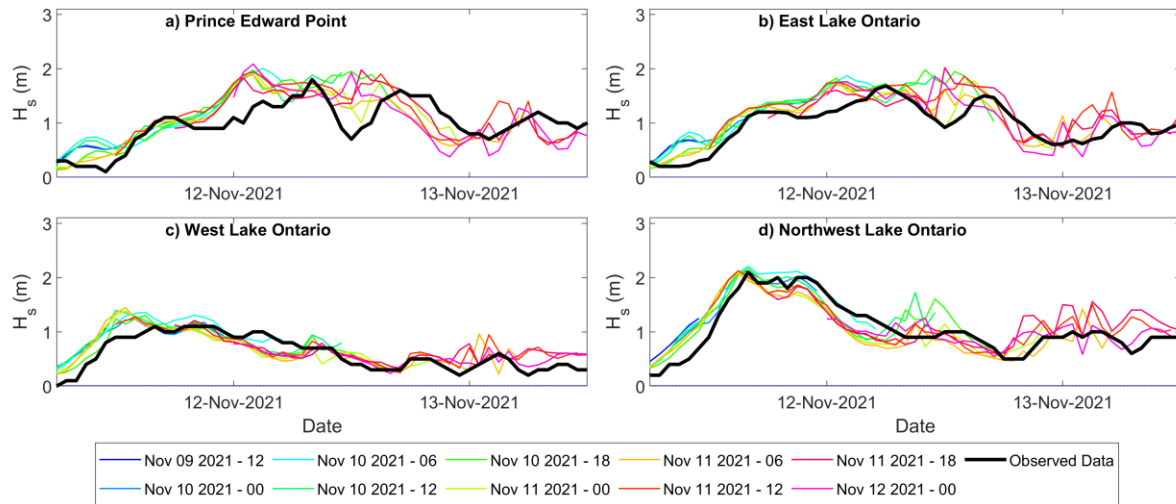


315
 316 **Figure 6:** Contour plots showing maps of modelled water levels at the peak of the storm event from two
 317 different forecasts, with an a) 35 hr lead time starting November 11, 00:00 UTC and b) 11 hour lead time
 318 starting on November 12, 00:00 UTC, with observed data plotted at the observation locations in black
 319 circles. Panels c) to h) show metrics including the RE and RMSE for peak storm surge magnitude at the
 320 locations of 6 selected water level gauges from the 8 forecasts preceding the storm event.

321
 322 Measured waves during this event reached up to 2.10 m, with the buoys in the western region of the lake
 323 (Fig. 7c, d) experiencing peak wave heights about 12 h earlier (Nov 11, 2021, 18:00 UTC) than the buoys
 324 in the eastern region of the lake (Fig. 7a, b; Nov 12 2021, 06:00 UTC). This is explained by the shift in
 325 wind direction over the storm duration, with winds originally from the southeast, rotating clockwise, then
 326 blowing dominantly from the west along the axis of the lake (Fig. S3 in the supplementary material).
 327 Overall, forecast simulations captured the magnitude of the waves all stations, with some error, and
 328 approximately 5 h delay in the timing of the peak H_s at Prince Edward Point (Fig. 7a). Error for waves
 329 during this event, at all stations, was constant for consecutive forecasts at all stations, with RMSE for

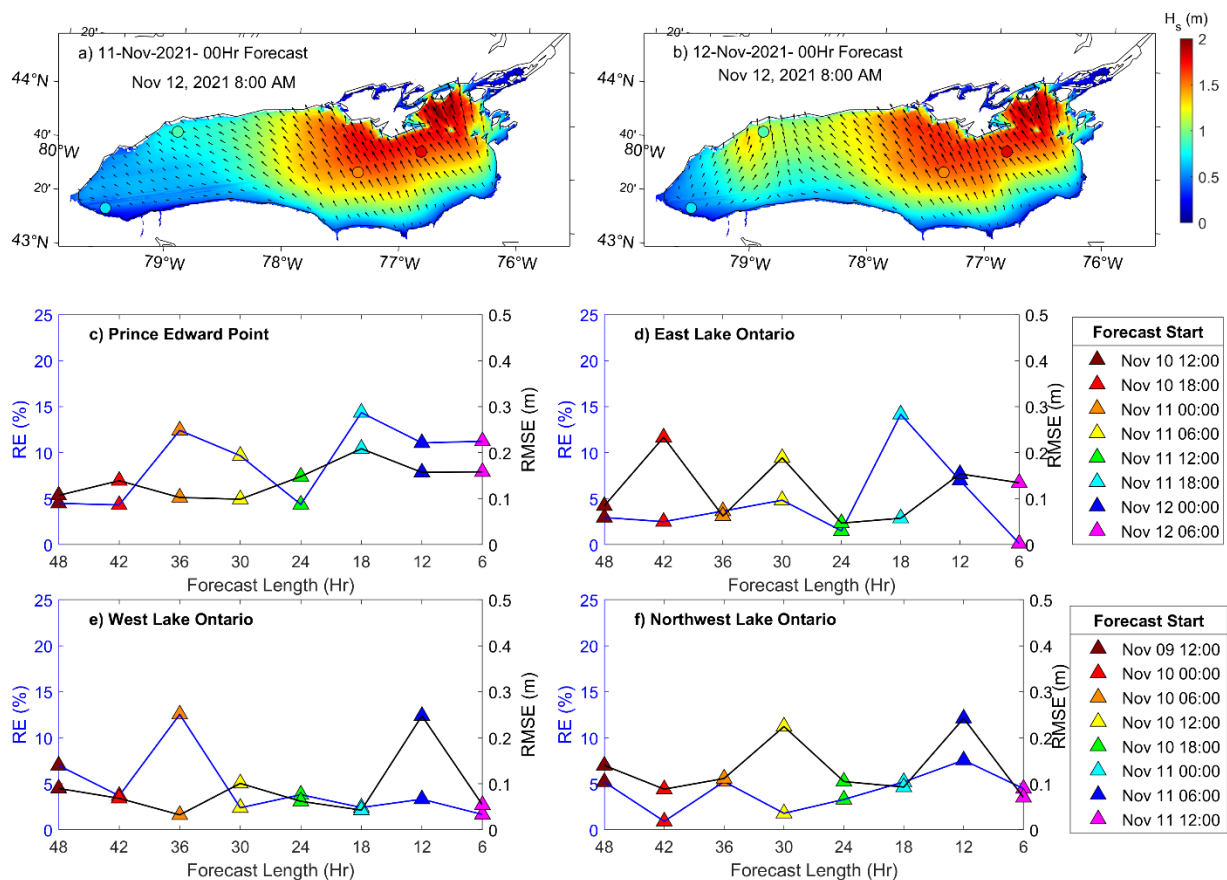
330 between 0.03 – 0.25 m and RE between 1-12%. Despite the generally consistent results, at the buoy
 331 locations, maps from different forecasts show distinct changes between the 36 h forecast (Fig. 8a) and the
 332 6 h forecast (Fig. 8b). Simulated wave fields in the northeast region of the lake showed similar results
 333 between forecasts, but in the northwest, predicted wave magnitudes and directions were distinctly different.
 334 The earlier forecast predicted waves under 0.70 m coming from the southeast, whereas the later forecast
 335 showed larger waves ($H_s = 0.50 - 1.00$ m) from the southwest, which can be attributed to changes in
 336 forecasted wind-fields.

337



338

339 **Figure 7:** Time series of measured H_s at the location of the 4 buoys compared to modelled data from
 340 progressive model forecasts for Event 1 (November 12, 2021).

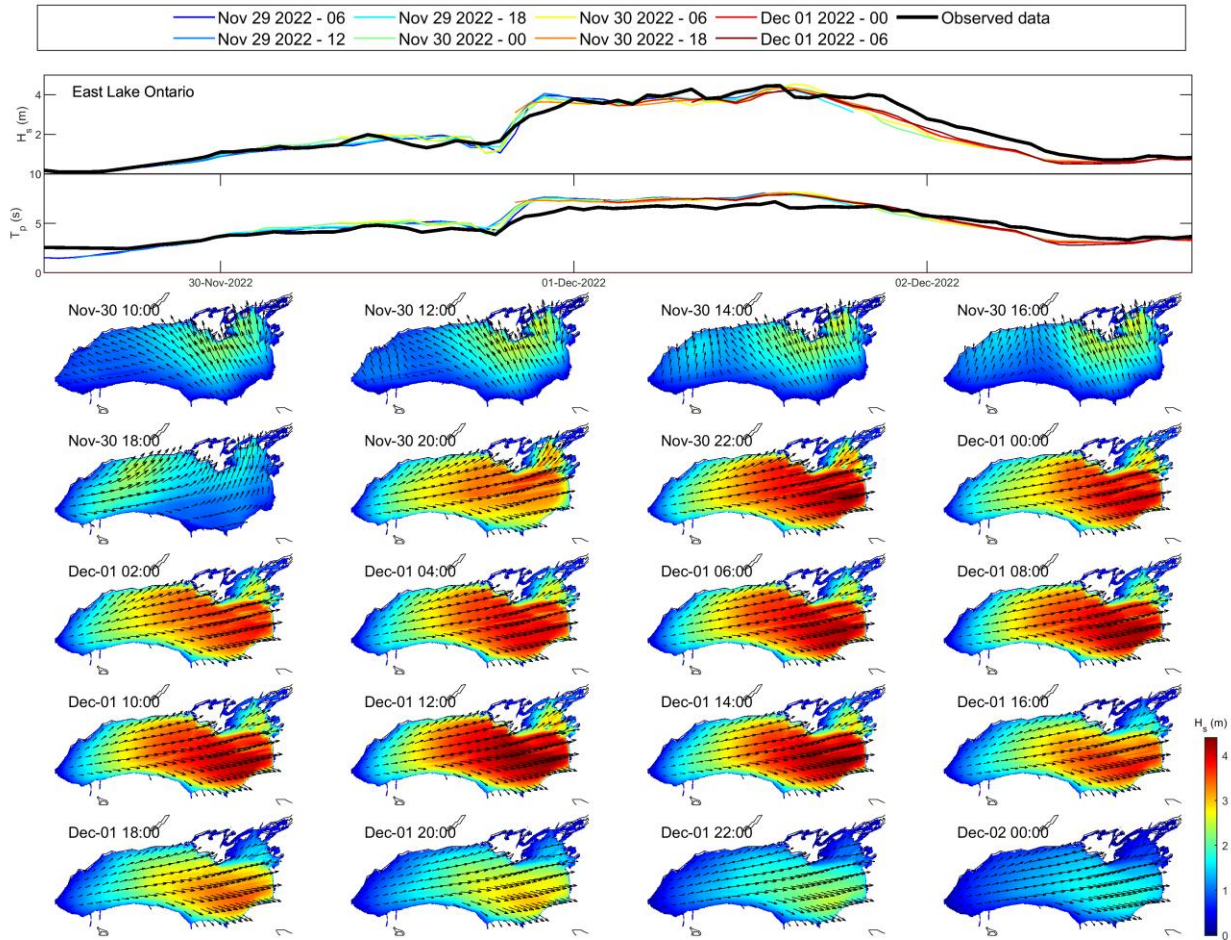


341
 342 **Figure 8:** Contour maps of modelled waves with vectors indicating wave direction at a select time during
 343 the storm event from two forecasts, with: a) 32 hr lead time starting November 11, 00:00 UTC; and b) 8 hr
 344 lead time starting November 12, 00:00 UTC with observed data plotted at the observation locations in black
 345 circles. Every 10th vector is plotted for clarity. Panels c) to f) show metrics including the RE and RMSE for
 346 significant wave height at the locations of 4 buoys from the 8 forecasts preceding the storm event on
 347 November 12, 2021, 12:00 UTC, and RMSE values are computed over a 12 h period centered at the time
 348 of the peak H_s for each station.

349
 350 For further investigation into model performance during storm events, wave forecasts during the event that
 351 resulted in the largest observed wave heights (December 1, 2022, Fig. 3c) were examined. During this
 352 storm, the lake experienced sustained easterly winds for almost 24 h, reaching speeds $> 20 \text{ m s}^{-1}$ on
 353 December 1, 14:00 UTC, generating waves $> 4 \text{ m}$ (Fig. 9). Data was only available from the one buoy at
 354 East Lake Ontario during this event, which recorded a maximum $H_s = 4.46 \text{ m}$. The forecasts initially
 355 underestimated this value, with a maximum predicted wave height of $H_s = 4.19 \text{ m}$ from the forecast starting
 356 on November 29 18:00 UTC, and the next forecast then overestimated this value ($H_s = 4.54 \text{ m}$). Subsequent

357 forecasts slightly underestimated the peak value, with the lowest predicted peak $H_s = 4.26$ m and the
 358 maximum values occurring ~ 1 h after the observed peak. All forecast results tended to overestimate the
 359 peak wave period, with predicted values ranging between 7.8 - 8.1 s, compared to an observed maximum
 360 value of 7.2 s.

361



362

363 **Figure 9:** Variability in significant wave height during a storm event: measured H_s compared to progressive
 364 forecast results at the Prince Edward Point Buoy for Event 3 (December 1, 2022; top) and maps of H_s and
 365 wave direction shown at an interval of 2 h (every 10th vector is shown for clarity).

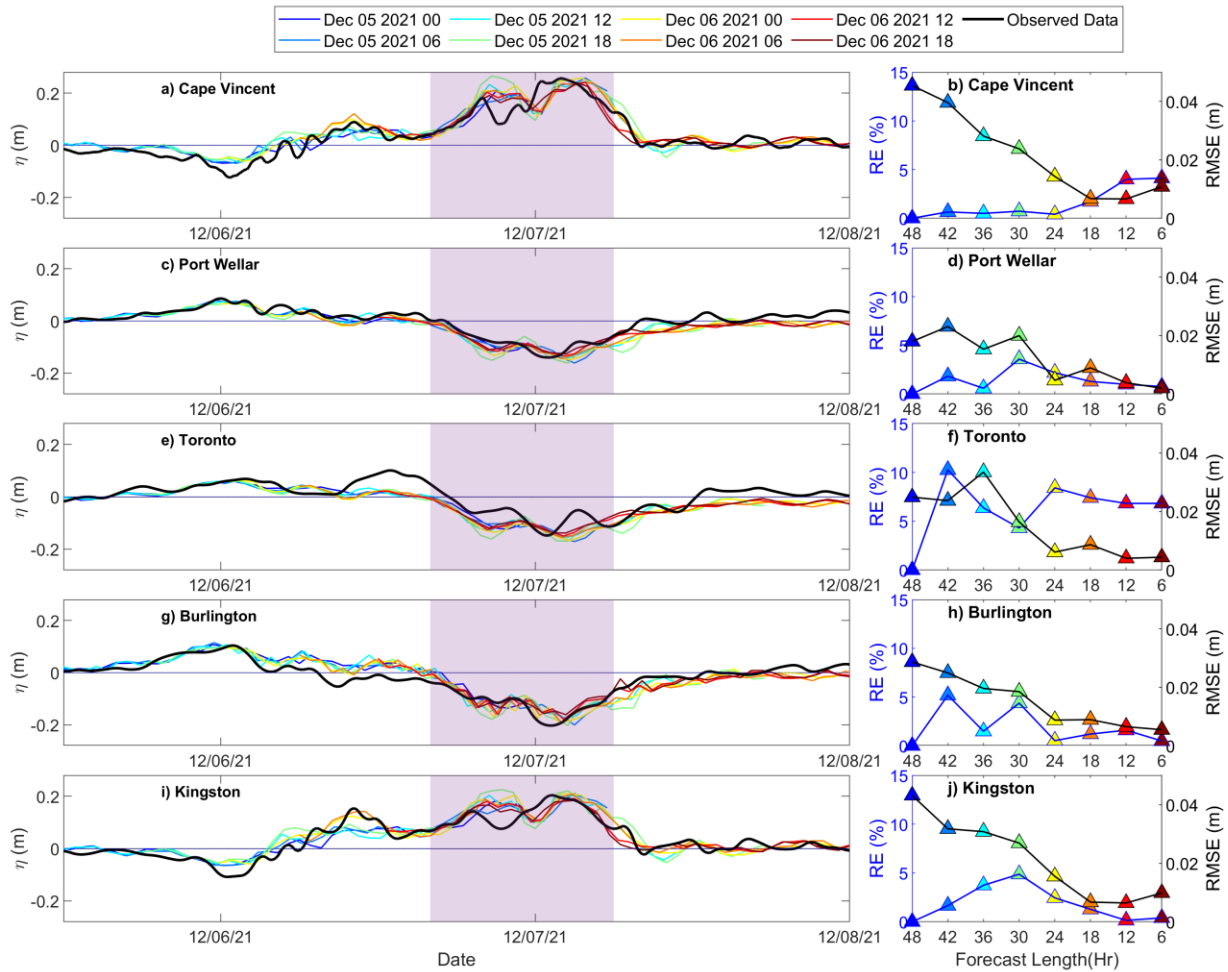
366

367 4 Discussion

368

369 4.1. Forecast Lead Times

370 Water level forecasts during a storm event on December 8, 2021, were examined in relation to forecast lead
 371 time. During this event, 21 m s^{-1} winds (Figure S4 in the supplementary material) generated a storm surge
 372 of approximately 0.20 m along the northeast coast, and a resulting setdown of 0.10 m on the opposite end
 373 of the lake. Error statistics throughout the peak of the event, as a function of forecast lead time, were plotted
 374 at selected stations (Fig. 10). The timing and magnitude of the storm surge was well represented by the
 375 forecast model, with $\text{RMSE} < 0.05 \text{ m}$ for all forecasts and a maximum $\text{RE} = 14\%$.
 376



377
 378 **Figure 10:** Time series of measured water levels at select observation points compared to forecasted data
 379 from progressive model simulations for Event 3: December 08, 2021, with corresponding plots showing
 380 computed RMSE calculated over the shaded area and percent error in peak storm surge from the 8 forecasts
 381 preceding the storm event.

382
 383 Trends in the error can be identified for this event at all stations, with notable patterns corresponding to
 384 locations with larger fluctuations in water level (i.e., Cape Vincent, Kingston, Burlington). At these sites,

385 forecast error tended to decrease as the forecast length shortened. At Cape Vincent, the initial 48 h forecast
386 had an RMSE of 0.05 m and by the 18 h forecast, the RMSE had decreased to 0.01 m. However, after the
387 18 h forecast there was a slight increase in RE from less than 1% to about 5% (Fig. 10b). Trends in
388 decreasing error were also observed at Kingston, where a similar decrease in RMSE was observed, and the
389 RE was maintained between 1 – 5%, corresponding to a maximum underprediction of about 0.05 m (Fig.
390 10i, j). The locations with smaller ranges in surface fluctuations (Toronto, Port Wellar) generally showed
391 constant error (0.02 m and ~1% at Port Wellar; 0.01 m and 7% at Toronto) for consecutive forecast results
392 over the duration of this event (Fig. 10d, f).

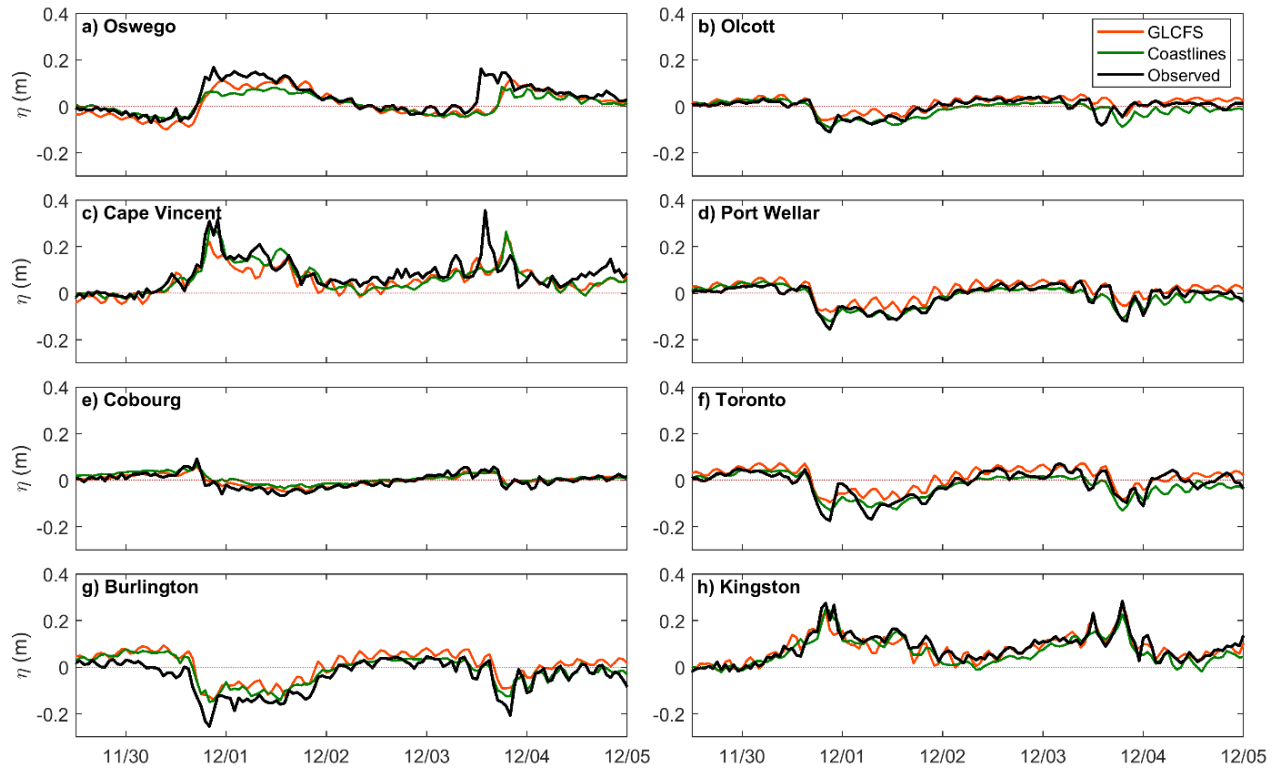
393
394 Hydrodynamics in the model are only driven by atmospheric forcing, which is a primary source of
395 uncertainty in simulations of surface dynamics in large lakes. The accuracy of meteorological forecasts
396 typically decreases with increasing length due to assimilation schemes using observations and satellite
397 imagery to yield more accurate results (Buehner et al., 2015). Therefore, it is expected that hydrodynamic
398 forecast simulations will increase in accuracy as the lead time to a storm event decreases. For forecasts of
399 storm surges in other Great Lakes (e.g., Lake Erie; Lin et al., 2022) and coastal seas (e.g., Gulf of Mexico;
400 Dietrich et al., 2018), improvements in storm surge predictions are directly linked to increased accuracy in
401 meteorological forcing leading up to an event. However, our Lake Ontario model results do not follow a
402 consistent trend between different events, either improving (Fig. 10) or maintaining accuracy (Fig. 6;
403 Fig. 8). Cases where error increases (i.e. Fig 10b) or remains constant (i.e. Fig. 8), can be explained due to
404 sources of uncertainty in the model calibration and neglecting additional hydrodynamic processes in the
405 model setup (i.e. 3-dimensional circulation). Despite model accuracy being constant at the observation
406 locations, changes in the spatial variability of predicted water levels and wave conditions for different
407 forecasts are not clearly communicated through time series analysis but are qualitatively shown in maps of
408 results (Fig. 6; Fig. 10).

409
410 *4.2. Comparison with Other Models*

411 The current work (Coastlines-LO) makes use of a relatively simple, low computational demand modelling
412 approach. The performance of this model can be compared to the GLCFS, which delivers a higher resolution
413 and more complex forecast system in throughout the Great Lakes. Differences between predictions from
414 these models can be explained according to the setup of each system, including different hydrodynamic
415 models, grid resolutions, and atmospheric forcing inputs, which are summarized in table S3 in the
416 supplementary material. The GLCFS uses the 2 km horizontal resolution High Resolution Rapid Refresh
417 (HRRR) meteorological forcing, which is comparable to HRDPS (2.5 km), however previous studies have
418 found that wind and direction predictions can vary between these models (Rey and Mulligan, 2021;

419 Swatridge et al., 2022). The inclusion of waves in the two systems is also accounted for differently, with a
420 separate model (WaveWatch III) used to simulate waves in the GLCFS, while Coastlines-LO uses a
421 dynamically coupled wave and flow model that accounts for wave-current interactions. The inclusion of
422 wave coupling in simulations of the Great Lakes can impact water level predictions (Mao and Xia, 2017).
423 The GLCFS runs on NOAA's high performance computing system, and the larger computational power
424 allows it to include 3D baroclinic processes while still running in the required timeframe, whereas the
425 Coastlines-LO system in the present study uses a 2D, depth averaged approach, and therefore doesn't
426 resolve vertical gradients in lake temperature or 3D circulation. The inclusion of river inflows and outflows
427 in the GLCFS also allows the model to simulate seasonal changes in the mean lake water level instead of
428 accounting for these changes based on observed data in post-processing.

429
430 Forecasts results from both models were compared to observed data over a 6-day period in December 2022,
431 during which 2 storm events occurred (Fig. 11; Table S4 in the supplementary material). Results from the
432 first 6 h of subsequent forecasts are combined to construct a water level time series at observation points
433 for both models for the entire duration. Both models represent trends in water levels over this, resulting in
434 comparable metrics, with an average RMSE 0.02 m for both models, and $r = 0.73$ and 0.74 for Coastlines-
435 LO, and GLCFS, respectively. GLCFS achieved better predictions of peak water levels at Oswego for the
436 event on December 1 (RE = 30% for GLCFS, RE = 51% for Coastlines-LO; Fig. 11a), and more accurately
437 represented the surface fluctuations observed over the entire 6 day period at Toronto (Fig. 11f). While
438 GLCFS was able to represent water levels at some locations, Coastlines-LO had higher accuracy predictions
439 at others (Fig. 11c, d). At Port Wellar and Cape Vincent, Coastlines-LO better predicted the peak set-down
440 and set-up on December 1 by 0.01 m and 0.03 m respectively, while GLCFS underpredicted at these
441 locations by 0.05 m and 0.09 m. Both models had difficulty simulating the second storm surge (December
442 3) at Oswego and Cape Vincent (Fig. 11 a, c), where the observed surge occurs approximately 3 h before
443 the predicted peak. At the Kingston station (Fig. 11h), storm surges of 0.25 m and 0.30 m are observed.
444 Coastlines-LO yielded better predictions for the first event, simulating a peak value of 0.24 m, compared
445 to 0.28 m predicted by GLCFS, while GLCFS performed better for the second event, with a predicted storm
446 surges of 0.28 m and 0.22 m for GLCFS and Coastlines-LO, respectively. Therefore, while the GLCFS
447 offers several advantages, Coastlines-LO provides comparable results for water level prediction with a
448 lower computational demand. This demonstrates that a relatively simple modelling system can be applied
449 to coastal environments to achieve accurate and efficient hydrodynamic predictions. The open-source and
450 flexible wrapper code could therefore be theoretically adapted to include different hydrodynamic models
451 and investigate different field sites as previous works have successfully applied similar approaches for
452 forecast modelling (e.g., Lin et al., 2022; Rey and Mulligan 2021).



453
 454 **Figure 11:** Compiled Coastlines-LO forecast results compared to forecasts from the GLCFS and observed
 455 data at select water level gauge locations interpolated to a 30 minute time resolution for 2 subsequent events
 456 between November 30 – December 5, 2022.

457 *4.3. Limitations and Uncertainties*

458 Sensitivity testing and calibration of the numerical model this system is based on, comes from the work of
 459 Swatridge et al. (2022), which found that 3D simulations of Lake Ontario improved predictions of surface
 460 behaviour compared to 2D depth averaged simulations. The 3D simulation allowed the model to account
 461 for transfer of surface momentum into baroclinic motions, giving a better representation of current
 462 velocities and surface seiching following a storm event, resulting in reduced RMSE during storm events by
 463 up to 12%, and improvement in modelled peak storm surge magnitude by up to 0.03 m. While 3D
 464 simulations improved accuracy, they also increased the computational runtime of a 24 h simulation from
 465 about 2.5 h to 4 h. Ten-day forecasts of 3D hydrodynamic processes in Lake Erie has been achieved by Lin
 466 et al. (2022) in using the AEM3D model with a similar Coastlines computational workflow as the current
 467 work; however, the Lake Erie model is on a coarser 2 km horizontal grid and does not couple with SWAN
 468 to predict surface waves, which is computationally expensive compared to hydrodynamic simulations.
 469 Therefore, to apply this model in real-time with a new simulation every 6 h, 2D simulations are used,
 470 potentially resulting in up to 12% greater uncertainty in the forecast results. Additional investigation of

471 real-time model performance during more storm events, including when the lake is stratified is
472 recommended for further model validation.

473
474 There is additional uncertainty in model results during the winter season, when ice forms in the Great Lakes.
475 Lake Ontario typically experiences some ice cover between December and April (Anderson et al., 2018),
476 which impacts lake processes, including water levels, circulation, and waves through limited air-water
477 momentum transfer (Anderson et al., 2018; Farhadzadeh and Gangai, 2017). While ice cover has been
478 simulated in Lake Ontario using other models (e.g., Oveisy et al., 2012), it is presently not available in
479 Delft3D-SWAN. Therefore, simulations of surface behaviour during the ice-covered months would have
480 limited accuracy in ice-covered areas. Future work could incorporate ice cover into the model by applying
481 dynamic masking of ice-covered surfaces using satellite data to improve results during these months.

482
483 While this system requires low computational resources, making it flexible for adaption to other coastal
484 regions, its capability for forecasting in additional locations is an area that requires future investigation.
485 The applicability of the model is limited by the availability of online data for model forcing and validation.
486 In order to account for seasonal changes in mean lake levels, near real-time measurements of water levels
487 are needed in the simulation to adjust the datum in post-processing. However, if no data were available the
488 simulation could include the wind-generated short-term fluctuations in surface levels and real-time
489 operations could continue. The workflow of the model is also limited by the availability of atmospheric
490 forcing data, with any interruptions of service in the HRDPS forecasts causing the hydrodynamic
491 simulations to fail for that run-cycle. Improvements in the system could account for this by providing a
492 secondary source of atmospheric forcing in that case. In future studies, we recommend applying this system
493 to a region in the coastal ocean, therefore requiring the development of real-time forecast inputs of open
494 boundary conditions.

495

496 **5 Conclusions**

497
498 A forecast model for wind-driven hydrodynamics was developed and applied to Lake Ontario using an
499 approach with relatively low computational demand. Wind-waves and water levels were simulated using a
500 dynamically coupled Delft3D-SWAN model driven by high resolution atmospheric forcing. Simulations
501 were able to forecast the wind-driven variability in the lake surface, with seasonal changes in the total water
502 levels accounted for by adjusting the datum for each forecast cycle based on observations of the mean water
503 level. The system provides rapid (~5 h runtime) predictions that are publicly available through the project
504 webpage, with the automated system forecasting a 48 h period every 6 h. The model has been running

505 continuously since April 2021, capturing a variety of storm events with storm surges up to 0.30 m and
506 significant wave heights over 4.00 m. Reliable prediction for wave conditions during winter months are
507 provided by the forecast model when no wave observations are available, however accuracy is limited
508 where ice is present as this process is not included in the modelling system.

509
510 Results show that the model is effective in simulating short term fluctuations in the water levels and wave
511 conditions during strong storm events, with relative errors between observed and forecasted storm surge
512 magnitudes and significant wave heights of less than 15%. Larger errors typically corresponded to locations
513 in the lake with larger ranges in observed water levels. For storm events, as the forecast lead time decreases
514 for progressing forecasts, the simulated results changed as a result of updates to the meteorological forcing.
515 No constant trends in forecast error due to decreasing forecast length were apparent, with forecast accuracy
516 increasing with shorter forecasts in some cases and staying constant at others, but overall results agreed
517 well with observed data for all forecasts leading up to an event, with RMSE for storm surge and waves
518 below 0.05 m and 0.30 m, respectively. The model compared well with other existing forecast models in
519 the Great Lakes (GLCFS), yielding comparable results for water level predictions during multiple storm
520 events. Due to the low computational requirements and pan-Canadian coverage from the High Resolution
521 Deterministic Prediction System forecasts, this model could be adapted to other Canadian lakes and coastal
522 seas with available bathymetry data for storm surge prediction and monitoring.

523

524 **6 Code and Data Availability Statement**

525

526 Real-time model results are available at <https://coastlines.engineering.queensu.ca/lake-ontario/>, and
527 archived on the local server, to be made available by contacting the corresponding author. HRDPS input
528 data is available from the Meteorological Service of Canada Datamart and observed data is openly
529 accessible online, as cited in the text. The source code and documentation of the open source numerical
530 model (Delft3D 4.01.01) can be accessed on their online repositories
531 (<https://oss.deltares.nl/web/delft3d/source-code>, last access: 19 December, 2023). The Python and
532 MATLAB scripts, and supporting files used in the automated workflow, as well as data and scripts used
533 to generate the plots presented in this paper are archived on Zenodo
534 (<https://doi.org/10.5281/zenodo.10407863>, Swatridge, 2023).

535

536 **7 Author contributions**

537

538 The concept of the COASTLINES-LO workflow was designed by RM, LB, SS, and LS, and LS
539 implemented the idea. LS developed the performed the model simulations. All authors contributed to the
540 validation of the model and interpretation of the results. LS wrote the manuscript with contributions from
541 LB, SS, and RM.

542

543 **8. Competing Interests**

544

545 The contact author has declared that neither they nor their co-authors have any competing interests.

546

547 **9 Acknowledgments**

548

549 Funding for this research was provided by Natural Sciences and Engineering Research Council of Canada
550 (NSERC) under the Discovery Grant program awarded to R.P. Mulligan (RGPIN/04043-2018), and a
551 Queen's Dean's Research Fund award to L. Boegman, R.P. Mulligan and S. Shan.

552

553 **10. References**

554 Anderson, E. J., Fujisaki-Manome, A., Kessler, J., Land, G.A., Chu, P.Y., Kelley, J.G.W., Chen, Y., and
555 Wang, J.: Ice Forecasting in the Next-Generation Great Lakes Operational Forecast System
556 (GLOFS). *J. Mar. Sci. Eng.*, 6(4), 123, <https://doi.org/10.3390/jmse6040123>, 2018.

557 Asher, T.G., Luettich, R.A., Fleming, J.G., and Blandton, B.O.: Low frequency water level correction in
558 storm surge models using data assimilation. *Ocean Modelling*, 144,
559 <https://doi.org/10.1016/j.ocemod.2019.101483>, 2019.

560 Baracchini, T., Wuest, A., and Bouffard, D.: Meteolakes: An operational online three-dimensional
561 forecasting platform for lake hydrodynamics. *Water Research*, 172.1-12,
562 <https://doi.org/10.1016/j.watres.2020.115529>, 2020.

563 Bender, M.A., Knutson, T.R., Tuleya, R.E., Sirutis, J.J., Vecchi, G.A., Garner, S.T. and Held, I.M.:
564 Modeled impact of anthropogenic warming on the frequency of intense Atlantic hurricanes.
565 *Science*, 327(5964), 454-458, DOI: 10.1126/science.1180568, 2010.

566 Bilskie, M.V., Asher, T.G., Miller, P.W., Fleming, J.G., Hagen, S.C. and Luettich Jr. , R.A.: Real-time
567 simulated storm surge predictions during Hurricane Michael (2018), *Wea. Forecasting*, 37, 1085–
568 1102, <https://doi.org/10.1175/WAF-D-21-0132.1>, 2022.

569 Buehner, M., McTaggart-Cowan, R., Beaulne, A., Charette, C., Garand, L., Heilliette, S., et al.:
570 Implementation of Deterministic Weather Forecasting Systems Based on Ensemble-Variational

571 Data-Assimilation at Environment Canada. Part 1: The Global System, *Mon. Wea. Rev.*, 143,
572 2532–2559, <https://doi.org/10.1175/MWR-D-14-00354.1>, 2015.

573 Booij, N., Ris, R.C., and Holthuijsen, L.H.: A third-generation wave model for coastal regions: 1. Model
574 Description and validation. *Journal of Geophysical Research: Oceans*, 104(C4), 7649-7666,
575 <https://doi.org/10.1029/98JC02622>, 1999.

576 Carey, C.C., Woelmer, W.M., Lofton, M.E., Figueiredo, R.J., Bookout, B.J., Corrigan, R.S., et al.:
577 Advancing lake and reservoir water quality management with near-term iterative ecological
578 forecasting, *Inland Waters*, 12(1), 107-120, <https://doi.org/10.1080/20442041.2020.1816421>,
579 2022.

580 Chisholm, L., Talbot, T., Appleby, W., Tam, B., and Rong, R.: Projected change to air temperature, sea-
581 level rise, and storms for the Gulf of Main region in 2050, *Elem Sci Anth.* 9(1), 1-14,
582 <https://doi.org/10.1525/elementa.2021.00059>, 2021.

583 Cooper, A.H., and Mulligan, R.P.: Application of a Spectral Wave Model to assess Breakwater
584 Configurations at a small craft harbour on Lake Ontario, *J. Mar. Sci. Eng.*, 2016, 4(3), 46,
585 <https://doi.org/10.3390/jmse4030046>, 2016,

586 Danard, M., Munro, A., and Murty, T.: Storm surge hazard in Canada. *Natural Hazards*, 28, 407–434,
587 <https://doi.org/10.1023/A:1022990310410>, 2003.

588 Dietrich, J. C., Muhammad, M., Curcic, M., Fathi, A., Dawson, C. N., Chen, S. S., and Luettich Jr., A.:
589 Sensitivity of Storm Surge Prediction to Atmospheric Forcing during Hurricane Isaac, *J. Waterway,*
590 *Port, Coastal, and Ocean Eng.* 144(1), [https://doi.org/10.1061/\(ASCE\)WW.1943-5460.0000419](https://doi.org/10.1061/(ASCE)WW.1943-5460.0000419),
591 2018.

592 Elko, N., Dietrich, C., Cialone, M.A., Stockdon, H., Bilksie, M. W., Boyd, B., Charbonneau, B., Cox., D.,
593 Desback, K., Elgar, S., Lewis, A., Limber, P., Long, J., Massey, C., Mayo, T., McIntosh, K., Nadal-
594 Caraballo, N.C., Raubenheimer, B., Tomiczek, T., Wargula, A. E. (2019). Advancing the
595 understanding of storm processes and impacts. *Shore & Beach*, 87(1).

596 Farhadzadeh, A., and Gangai, J.: Numerical Modelling of Coastal Storms for Ice-Free and Ice-Covered
597 Lake Erie, *J. of Coastal Research*, 33(6), 1383-1396, <https://doi.org/10.2112/JCOASTRES-D-16-00101.1>, 2017.

599 FEMA: FEMA Great Lakes Coastal Guidelines, Appendix D.3 Update. FEMA, 2014.

600 Forbes, C., Luettich, R.A., Mattocks, C.A., and Westerink, J.J.: A retrospective evaluation of the storm
601 surge produced by Hurricane Gustav (2008): Forecast and hindcast results, *Wea. Forecasting*,
602 25(6), 1577–1602, <https://doi.org/10.1175/2010WAF2222416.1>, 2010.

603 Fleming, J.G., Fulcher, C.W., Luettich Jr., R.A., Estade, B.D., Allen, G., and Winer, H.S.: A real time storm
604 surge forecasting system using ADCIRC, Proceedings of the International Conference on Estuarine
605 and Coastal Modeling, [https://doi.org/10.1061/40990\(324\)48](https://doi.org/10.1061/40990(324)48), 2008.

606 Gallagher, G.W., Duncombe, R.K., and Steeves, T. M.: Establishing Climate Change Resilience in the
607 Great Lakes in Response to Flooding, Journal of Science Policy & Governance, 17(1),
608 <https://doi.org/10.38126/JSPG170105>, 2020.

609 Gronewold, A.D., and Rood, R.B.: Recent water level changes across Earth's largest lake system and
610 implications for future variability, J. of Great Lakes Research, 45(1), 1-3,
611 <https://doi.org/10.1016/j.jglr.2018.10.012>, 2019.

612 Gronewold, A.D., Fortin, V., Lofgren, B., Clites, A., Stow, C.A., and Quinn, F.: Coasts, water levels, and
613 climate change: A Great Lakes perspective, Climate Change, 120, 697-711,
614 <https://doi.org/10.1007/s10584-013-0840-2>, 2013.

615 Huang, A., Rao, Y.R., Lu, Y., and Zhao, J.: Hydrodynamic modelling of Lake Ontario: An intercomparison
616 of three models. Journal of Geophysical Research: Oceans, 115(C12), 1-16,
617 <https://doi.org/10.1029/2010JC006269>, 2010.

618 Kelley, J.G.W., Chen, Y., Anderson, E.J., Lang, G.A., and Xu, J.: Upgrade of NOS Lake Erie Operational
619 Forecast System (LEOFS) to FVCOM: Model Development and Hindcast Skill Assessment; NOS
620 CS 40, NOAA; NOAA Technical Memorandum, <http://doi.org/10.7289/V5/TM-NOS-CS-40>,
621 2018.

622 Lacke, M. C., Knox, J. A., Frye, J. D., Stewart, A. E., Durkee, J. D., Fuhrmann, C. M., & Dillingham, S.
623 M. (2007). A climatology of cold-season non convective wind events in the Great Lakes region.
624 Journal of Climate, 20(24), 6012-6022. <https://doi.org/10.1175/2007JCLI1750.1>

625 Lesser, G.R., Roelvink, J.A., and Stelling, G.S.: Development and validation of a three-dimensional
626 morphological model, Coastal Engineering, 51(8-9), 883-915,
627 <https://doi.org/10.1016/j.coastaleng.2004.07.014>, 2004.

628 Lin, S., Boegman, L., Shan, S., and Mulligan, R.P.: An automatic lake-model application using near real-
629 time data forcing: Development of an operational forecast workflow (COASTLINES) for Lake
630 Erie, Geosci. Model Dev, 15(3), 1331-1353, <https://doi.org/10.5194/gmd-15-1331-2022>, 2022.

631 McCombs, M.P., Mulligan, R.P., Boegman, L., and Rao, Y.R.: Modelling surface waves and wind-driven
632 circulation in eastern Lake Ontario during winter storms, J. Great Lakes Res., 40(3), 130-142,
633 <https://doi.org/10.1016/j.jglr.2014.02.009>, 2014a.

634 McCombs, M.P., Mulligan, R.P., and Boegman, L.: Offshore wind farm impacts on surface waves and
635 circulation in Eastern Lake Ontario, Coastal Engineering, 93, 32-39,
636 <https://doi.org/10.1016/j.coastaleng.2014.08.001>, 2014b.

637 Mao, M., and Xia, M.: Dynamics of wave-current-surge interactions in Lake Michigan: A model
638 comparison, *Ocean Modelling*, 110, 1-20, <https://doi.org/10.1016/j.ocemod.2016.12.007>, 2007.

639 Milbrandt, J.A., Belair, S., Faucher, M., Vallee, M., Carrera, M.L., and Glazer, A.: The Pan-Canadian High
640 Resolution (2.5 km) Deterministic Prediction System, *Weather and Forecasting*, 31(6), 1791-1816,
641 <https://doi.org/10.1175/WAF-D-16-0035.1>, 2016.

642 Oveysy, A., Boegman, L., and Imberger, J.: Three-dimensional simulation of lake and ice dynamics during
643 winter, *Limnol Oceanogr*, 57(1), 43-57, <https://doi:10.4319/lo.2012.57.1.0043>, 2012.

644 Paramygin, V.A., Sheng, Y.P., and Davis, J.R.: Towards the development of an operational forecast system
645 for the Florida coast, *J. Mar. Sci. Eng.*, 5(1), <https://doi.org/10.3390/jmse5010008>, 2017.

646 Paturi, S., Boegman, L., and Rao, Y.R.: Hydrodynamics of eastern Lake Ontario and the upper St. Lawrence
647 River, *J. Great Lakes Res.*, 38(4), 194-204, <https://doi.org/10.1016/j.jglr.2011.09.008>, 2012.

648 Peng, M., Zhang, A., Anderson, E.J., Lang, G.A., Kelley, J.G.W., and Chen, Y.: Implementation of the
649 Lakes Michigan and Huron Operational Forecast System (LMHOFS) and the Nowcast/Forecast
650 Skill Assessment, NOAA technical report NOS CO-OPS, 2019.

651 Prakash, S., Atkinson, J.F., and Green, M.L.: A semi-Lagrangian study of circulation in Lake Ontario, *J.*
652 *Great Lakes Res.*, 33(4), 774-790,
653 [https://doi.org/10.3394/0380-1330\(2007\)33\[774:ASSOCA\]2.0.CO;2](https://doi.org/10.3394/0380-1330(2007)33[774:ASSOCA]2.0.CO;2), 2007.

654 Rey, A.J.M., and Mulligan, R.P.: Influence of hurricane wind field variability on real-time forecast
655 simulations of the coastal environment, *Journal of Geophysical Research: Oceans*, 126(1), 1-20,
656 <https://doi.org/10.1029/2020JC016489>, 2021.

657 Shore, J.A.: Modelling the circulation and exchange of the Kingston Basin and Lake Ontario with FVCOM,
658 *Ocean Modelling*, 30(2-3), 106-114, <https://doi.org/10.1016/j.ocemod.2009.06.007>, 2009.

659 Sogut, D.V., Jensen, R.E., and Farhadzadeh, A.: Characterizing Lake Ontario Marine Renewable Energy
660 Resources, *Marine Technology Society Journal*, 53(2), 21-38,
661 <https://doi.org/10.4031/MTSJ.53.2.3>, 2019.

662 Steinschneider, S.: A hierarchical Bayesian model of storm surge and total water levels across the Great
663 Lakes shoreline – Lake Ontario, *J. Great Lakes Res.* 47(3), 829-843,
664 <https://doi.org/10.1016/j.jglr.2021.03.007>, 2021.

665 Studholme, J., Fedorov, A.V., Gulev, S.K., Emanuel, K., and Hodges, K.: Poleward expansion of tropical
666 cyclone latitudes in warming climates, *Nature geoscience*, 15, 14-18,
667 <https://doi.org/10.1038/s41561-021-00859-1>, 2022.

668 Swatridge, L.L., Mulligan, R.P., Boegman, L., Shan, S., and Valipour, R.: Coupled modelling of storm
669 surge, circulation, and surface waves in a large, stratified lake, *J. Great Lakes Res.*, 48(6), 1520-
670 1535, <https://doi.org/10.1016/j.jglr.2022.08.023>, 2022.